HHS Public Access

Author manuscript

Adv Mater. Author manuscript; available in PMC 2021 January 11.

Published in final edited form as:

Adv Mater. 2016 July ; 28(26): 5322–5329. doi:10.1002/adma.201600383.

Multifunctional Charge-Transfer Single Crystals through Supramolecular Assembly

Beibei Xu,
Department of Mechanical Engineering, Temple Materials Institute, Temple University, Philadelphia, PA 19122, USA

Zhipu Luo,
Synchrotron Radiation Research Section, Macromolecular Crystallography Laboratory, National Cancer Institute, Argonne National Laboratory, Argonne, IL 60439, USA

Andrew J. Wilson,
Department of Chemistry, Temple University, Philadelphia, PA 19122, USA

Ke Chen,
Department of Physics, Temple Materials Institute, Temple University, Philadelphia, PA 19122, USA

Wenxiu Gao,
School of Materials Science and Engineering, Nanjing University of Science Technology, Nanjing 210094, P.R.China

Guoliang Yuan,
School of Materials Science and Engineering, Nanjing University of Science Technology, Nanjing 210094, P.R.China

Harsh Deep Chopra,
Department of Mechanical Engineering, Temple Materials Institute, Temple University, Philadelphia, PA 19122, USA

Xing Chen,
Energy Systems Division, Argonne National Laboratory, Argonne, IL 60439, USA

Katherine A. Willets,
Department of Chemistry, Temple University, Philadelphia, PA 19122, USA

Zbigniew Dauter,
Synchrotron Radiation Research Section, Macromolecular Crystallography Laboratory, National Cancer Institute, Argonne National Laboratory, Argonne, IL 60439, USA

Shenqiang Ren
Department of Mechanical Engineering, Temple Materials Institute, Temple University, Philadelphia, PA 19122, USA

shenqiang.ren@temple.edu.

Supporting information

Supporting Information is available from the Wiley Online Library or from the author.

Organic molecular charge-transfer (CT) solids have attracted tremendous interest in contemporary materials science, where the charge, spin, and lattice degrees of freedom are all strongly entangled to promote new properties (superconductivity, ferroelectricity, quantum spin liquid state, etc.) for flexible and lightweight multifunctional materials. The CT complexes, consisting of electron donor and acceptor networks, have been designed such that the interactions between charge and spin can give rise to unusual functional ferroic features due to the presence of charge-spin composite orders.[1–10] Historically, the invention of each new kind of CT complex initiates a technological revolution. Among these functional molecules, tetrathiafulvalene (TTF)-based CT salts attract considerable attention for their ability to arrange in a stacked conformation with a high degree of charge transfer. For example, the organic conducting complex TTF-TCNQ (7,7,8,8-tetracyanoquinodimethane) has stimulated research in organic conductors, metal-insulator transition, photoconductors, and field-effect transistors, which have benefited greatly from TTF and its derivative-based CT complexes. [11–18] More recently, the CT interaction between TTF electron donor and acceptors has also led to the enormous surge in the field of molecular ferronics which mixes charge and spin degrees of freedom, such as ferroelectric TTF-CA (*p*-chloranil) and TTF-pyromellitic diimide CT complexes,[19,20] as well as multiferroic TTF-BA (*p*-bromanil) CT crystals.[19,21] The discovery of ferromagnetism in the tetrakis(dimethylamino) ethylene-C_{60} (TDAE-C_{60}) CT complex has stimulated the generation of C_{60}-based molecular magnets,[22] arising from buckyball orientational (merohedral) disordering induced spin order of C_{60} molecules.[23–26]

A variety of ubiquitous and emerging phenomena in molecular CT solids have so far been attributed to the molecular orbitals in the donor-acceptor units.[27] As an electron donor, TTF has an ability to donate two electrons and has a small ionization potential ($I = 6.95 \pm 0.1$ eV) due to π-electron conjugation interaction.[11,28] In addition, the lowest unoccupied molecular orbital of fullerene has the ability to simultaneously accept up to six electrons.[29] The crystallization of TTF and C_{60} is complex and typically involves covalently linking the individual components or extensive surface functionalization to improve their processability. Such strategies often deteriorate or contaminate carbon surfaces, thus compromising their electronic, optical, and magnetic properties.[30–34] Furthermore, even if one succeeds in obtaining crystals from such a combination, that does not guarantee the coexistence of electric and magnetic ordering within the organic network, because there is no control over the molecular packing arrangement and the interaction of delocalized electrons.[35]

Here, we report external stimuli-responsive multifunctionalities in molecular charge-transfer single crystals built by electron donor TTF and acceptor fullerene (C_{60}). The intermolecular contacts between asymmetric TTFs and multiorientational C_{60} molecules lead to spin and charge order within the crystal structure. These crystals are found to exhibit spontaneous and hysteretic polarization, potential-dependent luminescence, and magnetoelectric properties owing to the presence of spin-charge composite ferroic ordering in the long-range ordered TTF-C_{60} lattice solids. In combination with their relatively simple crystallization process and broad chemical flexibility, molecular charge-transfer crystals promote the material-by-design paradigm toward the development of multifunctional all-organic nanoferronics.

The segregated crystallization of a TTF-C_{60} complex forms a 3D CT network, which ultimately induces unusual multifunctional ferroic properties. Molecular chemistry provides a unique and promising way to assemble high-quality TTF-C_{60} CT crystals (TCCTs, $C_{60}^{\bullet-}$-$TTF^{\bullet+}$) of centimeter dimensions (Figure 1 a,b). The time-dependent growth process (Figure S12, Supporting Information) indicates a mass-transport controlled nucleation at the liquid-air-solid interface, where a unique evaporation-dependent growth leads to the layered structure of the TCCTs, as shown in Figure S11 of the Supporting Information. The stoichiometry between the TTF donor and C_{60} acceptor moieties significantly influences the molecular assembly and the subsequent morphology of TCCT solids, producing structures such as dendrites (the weight ratio of TTF:C_{60} at 1:3, Figure S4, Supporting Information), stacking sheets (2:3, Figure 1c), and plates (3:3, Figure 1d), respectively. Optimized stacking of TTF enables molecular assembly into densely packed TCCTs with large dimensions. Without C_{60} molecules, TTF-only crystals exhibit columnar shape caused by the considerable interaction along 1D stacks (Figure S7–S9, Supporting Information). Next, a detailed structure and chemical analysis of TCCTs was performed to correlate the structure and property relationships. Cross-sectional scanning electron microscopy (SEM) and energy-dispersive X-ray spectroscopy images reveal a uniform 3D faceted morphology of TCCTs with a homogeneous distribution of carbon and sulfur elements (Figure S11a, Supporting Information). As high-quality crystals are a prerequisite for investigating the structural and function relationship, we selected TCCTs of TTF: C_{60} (3:3) for our following studies.

Single-crystal diffraction data of TCCTs were collected at 100 K with a wavelength of 0.8 Å on a SER-CAT 22-BM beamline at Advanced Photon Source in Argonne National Laboratory. The TCCT crystal structure is triclinic in centrosymmetric space group $P\bar{1}$ with unit cell dimensions: a = 13.356(3) Å, b = 20.269(4) Å, c = 31.853(6) Å, α = 103.95(3)°, β = 91.70(3)°, and γ = 102.17(3)° (Figure 1e; Table S1, Supporting Information), where the asymmetric unit cell contains four C_{60}, four TTF, and four 1,2-dichlorobenzene (DCB) molecules. Figure 1f and Figure S14a (Supporting Information) show the projection of TTF-C_{60} crystal packing along the a- and b-axes, respectively. The C_{60} molecules display four main orientations and one of them, close to the middle of b cell edge (shown as sky-blue in Figure 1e) is disordered with relative occupancy 0.81 and 0.19 by rotating about 40° around one of the threefold axes of C_{60} (Figure 1g). The high occupancy part of the disordered fullerene is used for further discussion. This kind of orientation and disorder is related to the magnetism of TCCTs and will be discussed in the later section on magnetics. The C_{60} molecules can form a charge-transfer network among themselves with short intermolecular C···C distances in the range of 2.915–3.389 Å, which is less than twice the van der Waals radius of carbon (3.4 Å) (Figure S14c and Table S2, Supporting Information). There are only short C···S contacts between TTF molecules with the distance of 3.477 Å (Figure S14d and Table S2, Supporting Information) which is less than the sum of van der Waals radius of carbon and sulfur (3.5 Å). The five crystallographically nonequivalent TTF molecules are arranged in two sets nearly perpendicular to each other in the TCCT crystal structure with C_{60} molecules packed in between, exhibiting the segregated stacking pattern (Figure S14b, Supporting Information) and form different intermolecular contacts with the neighboring C_{60} molecules with the short contact distances of C(C_{60})···C(TTF) 3.019–3.386 Å and

C(C_{60})···S(TTF) 3.229–3.496 Å (Figure S14d,e and Table S2, Supporting Information). The different contact distances between TTF and C_{60}, as well as multiorientational ordering of C_{60} molecules, indicate a possible magnetic mechanism in TCCTs analogous to the correlation between intermolecular orientations and magnetic properties in TDAE-C_{60} system.[24,26] The segregated packing in the crystal and multiple intermolecular interactions promote the TCCTs as an excellent candidate for charge transfer.

The unique molecular packing of TCCTs generally leads to new optical properties. Crystallized TTF-C_{60} solids exhibit a broad absorption spectrum, including the charge-transfer band originating from the excited triplet state $^{T}C_{60}$* and the short intermolecular C···S contacts between TTF and C_{60} (Figure 2a; Figure S16, Supporting Information).[36,37] Applying an external electric potential across the crystal enables the modulation of photoluminescence (Figure 2b) from the TCCTs. Two physical processes compete in these experiments: one involving the recombination of excitons leading to the release of energy as light emission; the other being the dissociation of excitons across the molecular interface to form the CT state leading to a decrease of emission intensity. Applying an external electric potential to the TCCTs promotes the dissociation of excitons at the interface, leading to reduction of the luminescence. Moreover, by decrease the potential from 6 to 0 V, the emission intensity can be recovered showing a reversible behavior in a cycle of increase or decrease of the potential (Figure S17, Supporting Information). The scheme of angle-dependent photoluminescence measurements (polarized emission) is presented in Figure S15 of the Supporting Information, in which the excitation polarization is aligned with the long axis of the as-grown crystal. In this experiment, the applied field is aligned in the same direction as the excitation polarization, and a stronger effect on the luminescence is observed when the polarization analyzer is set parallel to the applied potential compared to when it is set perpendicular to the applied field. The inset of Figure 2b shows the ratio of the intensity of the emission at 90° to that at 0° and verifies that the emission is preferentially quenched along the direction of the applied potential due to more favorable exciton dissociation along that axis.

The electrical properties of TCCT solids were examined to reveal their transport characteristics. The expression for the resistance can be described as $R = AT^{-\alpha}$, where R is the electric resistance, A is a coefficient, T is temperature, and α is an exponential factor. The temperature-dependent resistivity ($\approx 10^2$ MΩ cm) of TCCTs suggests a preexponential term and semiconductor-like behavior in the temperature range between 80 K and room temperature (Figure S18a, Supporting Information); this cannot be fit by Mott and Efros-Shklovskii hopping or a Boltzmann-like activation. The observed behavior can be attributed to thermally excited excitons, leading to an increase in the density of charge carriers and subsequently enhanced mobility of TCCTs. The conductivity and surface morphology of $TCCT_S$ were investigated by using atomic force microscopy (AFM) and conducting-AFM, which reveals the surface and transport properties of TCCTs (Figure S18b, Supporting Information). Magnetic responses of TCCTs provide a unique way to tune and control optical and electronic properties of organic CT complexes. Under a small external magnetic field (≈100 mT), the competition between spin-conserving and spin-mixing modifies the formation rate of spin-parallel and spin-antiparallel states, leading to the density change of singlet and triplet CT. This ultimately changes the photoluminescence intensity, namely the

magneto-photoluminescence of TCCTs (Figure 2c). The decrease of emission intensity under an external magnetic field further confirms the singlet to triplet conversion. Besides, under light illumination, current density increases indicating that the photoresponse of TCCTs is due to the dissociation of photogenerated excitons into free charges (Figure S18c, Supporting Information). To further explain the observed magnetic field effects and photoresponse character, magnetoconductance (MC) measurements were carried out. MC = $[J(B) - J(0)]/J(0)$, where J(B) and $J(0)$ refers to the current density with and without a magnetic field, respectively (the inset of Figure 2c,d; Figure S19 and S20, Supporting Information). A positive MC effect is shown, which results from an increased charge density due to the interaction between excitons and polarons[38] The MC effect could be further increased by the enhanced density of CT under photoexcitation (the inset of Figure 2c). In addition, an external electric field increases the charge density. This leads to an enhanced interaction between triplet excitons and polarons,[39] which, at a low electric field, results in an increase in the density of charge carriers for the positive MC (Figure 2d). However, on further increasing the electric field, the scattering interaction of polarons by the triplet excitons is largely enhanced, leading to the decrease of charge carrier mobility and a decrease in MC (Figure 2d). As shown in Figure 2c, a magnetic field can induce the singlet to triplet conversion. This ultimately leads to enhanced charge carrier density and an increase in positive MC (Figure 2d). As a result, the MC reaches the maximum value of 10.7% under an electric field of 40 kV cm^{-1} and a magnetic field of 400 mT.

The polarization and dielectric properties of TCCTs were examined to elucidate the CT effect on their ferroic properties, as shown in Figure 3. Room-temperature polarization hysteresis loop shows an obvious ferroelectric characteristic (Figure S21b, Supporting Information). Piezoresponse force microscopy (PFM) was used to obtain the local domain switching characteristics of TCCTs (Figure 3a–d; Figure S22, Supporting Information). Figure 3a shows a 30 × 30 μm^2 PFM phase image, in which the application of a 54 kV cm^{-1} voltage polarizes the center area of 20 × 20 μm^2. In contrast to Figure 3a, an opposite distinct domain with the size of 10 × 10 μm^2 can be found at the center after the application of −72 kV cm^{-1} voltage pulse. The consecutive poling of ferroelectric domain by a voltage pulse of −45, 10, and 90 kV cm^{-1} in Figure S22 (Supporting Information) also verifies the domain switching characteristic of TCCTs (Figure S22b–d, Supporting Information). To confirm the ferroelectric properties, the phase hysteresis loop and butterfly shape amplitude loop are also demonstrated with polarization switching by the tuning of tip bias (Figure 3c–d). The positive-up-negative-down measurement method (PUND, the inset of Figure 3c) further confirms the existence of remnant polarization in TCCTs. In addition, external stimuli could be utilized to control dielectric properties of TCCTs (Figure 3e–f). The enhanced permittivity with increasing temperature results from thermal excitation of triplet excitons. The inset of Figure 3c shows how the permittivity changes with temperature at 100 Hz according to $\frac{\Delta\varepsilon}{\varepsilon} = \frac{\varepsilon_{ex} - \varepsilon}{\varepsilon}$, where ε is the original permittivity without external stimuli, ε_{ex} is the modified permittivity after external stimuli (such as thermal excitation, photoexcitation, or magnetic field effects). The detailed temperature-dependent dielectric constant change is shown in Figure S21a (Supporting Information), suggesting that ferroelectric phase exists at room temperature.[40] Similar to the magnetic field effects shown in Figure 2, spin mixing leads to the conversion from singlet to triplet CT, and

consequently increases the density of triplet excitons (dipoles).[41] Thus, the permittivity and polarization of TCCTs simultaneously exhibit magnetic-field and light-illumination-dependent behavior (Figure 3f and the inset).

Electron spin resonance (ESR) is critically important for investigating the CT characteristic of TCCTs (Figure S23, Supporting Information). In addition to the C_{60}^- radical anion and TTF^+-related radicals (Figure S23a, Supporting Information),[36,42] another resonance peak emerges in the TCCTs, signaling the existence of CT. The CT-induced resonance of TCCTs also exhibits a strong light-intensity correlation with magnetic susceptibility (Figure S23c, Supporting Information).[43] The increase in light intensity induces an increase in the density of CT states and triplet excitons in the crystals, which leads to an increase in spin susceptibility.[43,44] Furthermore, electric field and photoexcitation can increase the magnetization due to increased density of CT in TCCTs (Figure 4a). The strong coupling between spin order and buckeyball orientation order exists within C_{60} molecules, where spin-spin interaction originates from the π-electron exchange interaction between neighboring C_{60} molecules induced by merohedral disorder.[26] As shown in Figure 4b, the orientations related to ferromagnetism (FM) and paramagnetism (PM) are shown by projecting the structure of C_{60} molecules along 010 direction. When the 6–6 double bond of C_{60} molecule faces the center of pentagon ring or hexagon ring of the neighboring C_{60} molecule, the spin interaction leads to FM or PM, respectively.[23] The temperature-dependent magnetization hysteresis loops suggest a thermal-excitation enhanced triplet CT state (Figure S25a, Supporting Information), in agreement with temperature-dependent polarization and permittivity (Figure 3e and S21a, Supporting Information). In addition, angle-dependent saturation magnetization shows the anisotropic magnetization behavior (Figure S24, Supporting Information), which results from electron-phonon (charge-lattice) coupling, induced narrow (wide) spin cone alignment along the magnetic easy (hard) axis.[45] With $S = 1/2$, this corresponds to a spin density of 0.09%. The TCCT solids not only show ferroelectric and magnetic properties, but also exhibit the magnetoelectric coupling effect. Figure S26a of Supporting Information demonstrates the magnetic-field-dependent ferroelectric characteristic of TCCTs, where magnetic-field-induced singlet to triplet conversion leads to an increase in triplet exciton (dipole) density and ultimately the polarization of TCCTs. The optimum magnetoelectric coupling coefficient of 760 mV cm^{-1} Oe^{-1} is achieved under an external electric field of 80 kV cm^{-1} and a magnetic field of 200 mT, as shown in Figure S26a of the Supporting Information. The mechanism of magnetoelectric coupling is illustrated in Figure 4c,d. Through CT interaction across the interface between TTF and C_{60}, electrons and holes are generated to occupy the bonding and anti-bonding molecular orbitals. Thus, the distribution of charges becomes unbalanced along the molecular chains leading to the generation of electric dipoles and spins, contributing to the generation of ferroic orders. This distribution of charges with electric dipoles and spins through the CT interaction is critical for the magnetoelectric coupling. Any change of the charge distribution will have a corresponding influence on the electric dipoles and spin of TCCTs. As shown in Figure 3h, the application of an electric field can enhance electric dipoles and spin, leading to the enhancement of magnetoelectric coupling effect.

In conclusion, multifunctional charge-transfer single crystals are developed by cocrystallization and segregated packing of electron donor TTF and acceptor C_{60} molecules,

forming a long-range ordered charge-transfer network. The unique molecular packing and diverse orientations of fullerene molecules within the crystal leads to an unusual multitude of external-stimuli-controlled ferroic properties, resulting from the modulation of the charge-spin composite orders. It should also be noted that the TCCTs exhibit light-controlled ferroic properties, as well as a large magnetoconductance of 10.7%. The findings presented here demonstrate the new and intriguing potentials of molecular charge-transfer solids for the development of multifunctional molecular ferronic materials.

Experimental Section

The detailed preparation methods for the crystals and devices, crystal structure details are provided in the Supporting Information based on the experimental data of synchrotron single-crystal diffraction pattern at 100 K. CCDC 1449048 contains the supplementary crystallographic data for this paper. These data can be obtained free of charge from The Cambridge Crystallographic Data Centre via www.ccdc.cam.ac.uk/data_request/cif.

Angle-dependent fl uorescence measurements were taken on an Olympus IX73 inverted microscope with a Princeton Instruments ACTON SpectraPro 2500i/Spec-10 spectrometer using a 20× objective to collect the fl uorescence. 4.3 μW of a 532 nm laser was used as the excitation source. The excitation laser was polarized parallel to the longer dimension of the crystal. In the detection path, a linear polarizer was varied between 0° (parallel to the excitation polarization) and 90° (perpendicular to it). The crystals were grown on indium tin oxide (ITO) glass substrates for electrical measurements. Electrodes were attached to the ITO substrate using silver epoxy and a Power Designs Inc. Model TP325 triple output DC power supply was used to modulate the applied potential from 0 to 6 V.

Conducting atomic force microscopy with topography and current images on the surface of the cocrystals were obtained by Bruker dimension icon atomic force microscopy. An Si probe coated with Cr/Pt on both sides with a radius below 25 nm was used. The resonant frequency of the probe was 13 kHz. The force constant of the probe was 0.2 N m^{-1}. The applied voltage was ≈5–10 V.

F or electrical properties related measurement, silver paste was patterned on both ends of the crystals as the electrode for Ohmic contact. MC measurement was taken by CHI-422 Series electrochemical workstation. Polarization hysteresis loops and PUND were carried out on Radiant Precision Premier II at 1000 Hz. An atomic force microscope equipped with Co/Cr-coated conductive tip was used to carry out PFM measurements (Brucker Multimode 8, Camarillo, CA, USA). Electron spin resonance signal and spin susceptibility was collected by Bruker EMX (type:ER073) plus ESR spectrometer. Magnetic hysteresis loops (M-H loop) were obtained by MicroSense EV7 vibrating sample magnetometer. For the M-H loop measurement, the crystals were bonded on a glass substrate with the crystalline long axis parallel to the magnetic field orientation as 0°. For the 90° of M-H loop, the crystalline long axis was vertical to the magnetic field orientation. The magnetoelectric coupling was measured with the crystalline long axis parallel to the magnetic field orientation.

Supplementary Material

Refer to Web version on PubMed Central for supplementary material.

Acknowledgements

Work at Temple University (S.R.) was supported by the Army Research Office, Young Investigator Program (W911NF-15-1-0610, material design/self-assembly of carbon photovoltaics), and the U.S. Department of Energy, Basic Energy Sciences Award No. DE-FG02-13ER46937 (organic synthesis and physical property measurement). Work at Temple University (A.J.W. and K.A.W.) was supported by the Department of Energy (DOE), Office of Science, Basic Energy Science (BES) under Award No. DE-SC0010307. H.D.C. gratefully acknowledges support from the National Science Foundation DMR, Condensed Matter Physics under Grant No. 1541236 (previously Grant No. 1309712) and Temple University's OVPR's Infrastructure Grant. Diffraction data were collected at the SER-CAT beamline 22BM at the Advanced Photon Source, Argonne National Laboratory. Use of the Advanced Photon Source was supported by the U.S. Department of Energy, Office of Science, Office of Basic Energy Sciences, under Contract No. W-31-109-Eng-38. The authors also thank Temple Materials Institute and Dr. X. Xi for the AFM measurements.

References

[1]. Alves H, Molinari AS, Xie H, Morpurgo AF, Nat. Mater. 2008, 7, 574. [PubMed: 18552852]

[2]. Kobayashi K, Horiuchi S, Kumai R, Kagawa F, Murakami Y, Tokura Y, Phys. Rev. Lett. 2012, 108, 237601. [PubMed: 23003988]

[3]. Miller JS, Epstein AJ, William MR, Chem. Rev. 1988, 88, 201.

[4]. Alves H, Pinto RM, Maçôoas ES, Nat. Commun. 2013, 4, 1842. [PubMed: 23673627]

[5]. Ren S, Wuttig M, Adv. Mater. 2012, 24, 724. [PubMed: 22213111]

[6]. Enoki T, Miyazaki A, Chem. Rev. 2004, 104, 5449. [PubMed: 15535656]

[7]. Liu H, Zhao Q, Li Y, Liu Y, Lu F, Zhuang J, Wang S, Jiang L, Zhu D, Yu D, Chi L, J. Am. Chem. Soc. 2005, 127, 1120. [PubMed: 15669849]

[8]. Lunkenheimer P, Müller J, Krohns S, Schrettle F, Loidl A, Hartmann B, Rommel R, de Souza M, Hotta C, Schlueter JA, Lang M, Nat. Mater. 2012, 11, 755. [PubMed: 22886065]

[9]. Hitoshi M, Acc. Chem. Res. 2013, 46, 248. [PubMed: 23128042]

[10]. Bushby RJ, Gooding D, Vale ME, Phil. Trans. R. Soc. A 1999, 357, 2939.

[11]. Toshiaki E, Akira M, Chem. Rev. 2004, 104, 5449. [PubMed: 15535656]

[12]. Craven RA, Salamon MB, Depasquali G, Herman RM, Stucky G, Schultz A, Phys. Rev. Lett. 1974, 32, 769.

[13]. Bright AA, Garito AF, Heeger AJ, Phys. Rev. B 1974, 10, 1328.

[14]. Tsutsumi J, Yamada T, Matsui H, Haas S, Hasegawa T, Phys. Rev. Lett. 2010, 105, 226601. [PubMed: 21231409]

[15]. Odom SA, Caruso MM, Finke AD, Prokup AM, Ritchey JA, Leonard JH, White SR, Sottos NR, Moore JS, Adv. Funct. Mater. 2010, 20, 1721.

[16]. Palmisano FZ, Centonze PGD, Quinto MA, Anal. Chem. 2002, 74, 5913. [PubMed: 12498183]

[17]. Sakai M, Sakuma H, Ito Y, Saito A, Nakamura M, Kudo K, Phys. Rev. B 2007, 76, 045111.

[18]. Ferraris J, Cowan DO, Walatka V, Perlstein JH, J. Am. Chem. Soc. 1973, 95, 948.

[19]. Kagawa F, Horiuchi S, Tokunaga M, Fujioka J, Tokura Y, Nat. Phys. 2010, 6, 169.

[20]. Tayi AS, Shveyd AK, Sue AC, Szarko JM, Rolczynski BS, Cao D, Kennedy TJ, Sarjeant AA, Stern CL, Paxton WF, Wu W, Dey SK, Fahrenbach AC, Guest JR, Mohseni H, Chen LX, Wang KL, Stoddart JF, Stupp SI, Nature 2012, 488, 485. [PubMed: 22914165]

[21]. Saito G, Murata T, Phil. Trans. R. Soc. A. 2008, 366, 139. [PubMed: 17846015]

[22]. Makarova TL, Sundqvist B, HoÈhne R, Esquinazi P, Kopelevichk Y, Scharff P, Davydov VA, Kashevarova LS, Rakhmanina AV, Nature 2001, 413, 716. [PubMed: 11607027]

[23]. Narymbetov B, Omerzu A, Kabanov VV, Tokumoto M, Kobayashi H, Mihailovic D, Nature 2000, 407, 883. [PubMed: 11057661]

[24]. Lappas A, Prassides K, Vavekis K, Arcon D, Blinc R, Cevc P, Amato A, Feyerherm R, Gygax FN, Schenc A, Science 1995, 267, 1799. [PubMed: 17775807]

[25]. Qin W, Gong M, Chen X, Shastry TA, Sakidja R, Yuan G, Hersam MC, Wuttig M, Ren S, Adv. Mater. 2015, 27, 734. [PubMed: 25389110]

[26]. Mihailovic D, Arcon D, Venturini P, Blinc R, Omerzu A, Cevc P, Science. 1995, 268, 400. [PubMed: 17746548]

[27]. Huth M, in Beilstein Bozen Symp. on Molecular Engineering and Control, (Eds: Hicks M, Kettner C), Beilstein Institut, Prien, Germany 2012, 121.

[28]. Garito AF, Heeger AJ, Acc. Chem. Res. 1974, 7, 232.

[29]. Xie Q, Perez-Cordero E, Echegoyen L, J. Am. Chem. Soc. 1992, 114, 3978.

[30]. Xiao J, Yin Z, Li H, Zhang Q, Boey F, Zhang H, Zhang Q, J. Am. Chem. Soc. 2010, 132, 6926. [PubMed: 20429506]

[31]. Farges JP, Brau A, Physica 1986, 143B, 324.

[32]. Sakai M, J. Appl. Phys. 2013, 113, 153513.

[33]. Ren L, Xian X, Yan K, Fu L, Liu Y, Chen S, Liu Z, Adv. Funct. Mater. 2010, 20, 1209.

[34]. Anzai H, J. Cryst. Growth. 1976, 33, 185.

[35]. Izuoka A, Tachikawa T, Sugawara T, Suzuki Y, Konno M, Saito Y, Shinohara H, J. Chem. Soc., Chem. Commun. 1992, 19, 1472.

[36]. Llacay J, Veciana J, Vidal-Gancedo J, Bourdelande JL, González-Moreno R, Rovira C, J. Org. Chem. 1998, 63, 5201.

[37]. Alam MM, Watanabe A, Ito O, J. Photochem. Photobiol. A 1997, 104, 59.

[38]. Qin W, Gong M, Shastry T, Hersam MC, Ren S, Sci. Rep. 2014, 4, 6126. [PubMed: 25146555]

[39]. Hu B, Yan L, Shao M, Adv. Mater. 2009, 21, 1500.

[40]. Liao W, Zhang Y, Hu C, Mao J, Ye H, Li P, Nat. Commun. 2015, 6, 7338. [PubMed: 26021758]

[41]. Qin W, Jasion D, Chen X, Wuttig M, Ren S, ACS Nano 2014, 8, 3671. [PubMed: 24654686]

[42]. Simonsen KB, Konovalov VV, Konovalova TA, Kawai T, Cava MP, J. Chem. Soc., Perkin Trans. 2 1999, 2, 657.

[43]. Qin W, Lohrman J, Ren S, Angew. Chem. Int. Ed. 2014, 53, 7316.

[44]. Ochsenbein ST, Feng Y, Whitaker KM, Badaeva E, Liu WK, Li X, Gamelin DR, Nat. Nano 2009, 4, 681.

[45]. Qin W, Chen X, Li H, Gong M, Yuan G, Grossman J, ACS Nano 2015, 9, 9373. [PubMed: 26257033]

[46]. Emsley P, Cowtan K, Acta Cryst. D 2004, 60, 2126. [PubMed: 15572765]

[47]. Macrae CF, Edgington PR, McCabe P, Pidcock E, Shields GP, Taylor R, J. Appl. Cryst. 2006, 39, 453.

[48]. Delano WL, The PyMOL Molecular Graphics System, DeLano Scientific LLC, San Carlos, USA 2002.

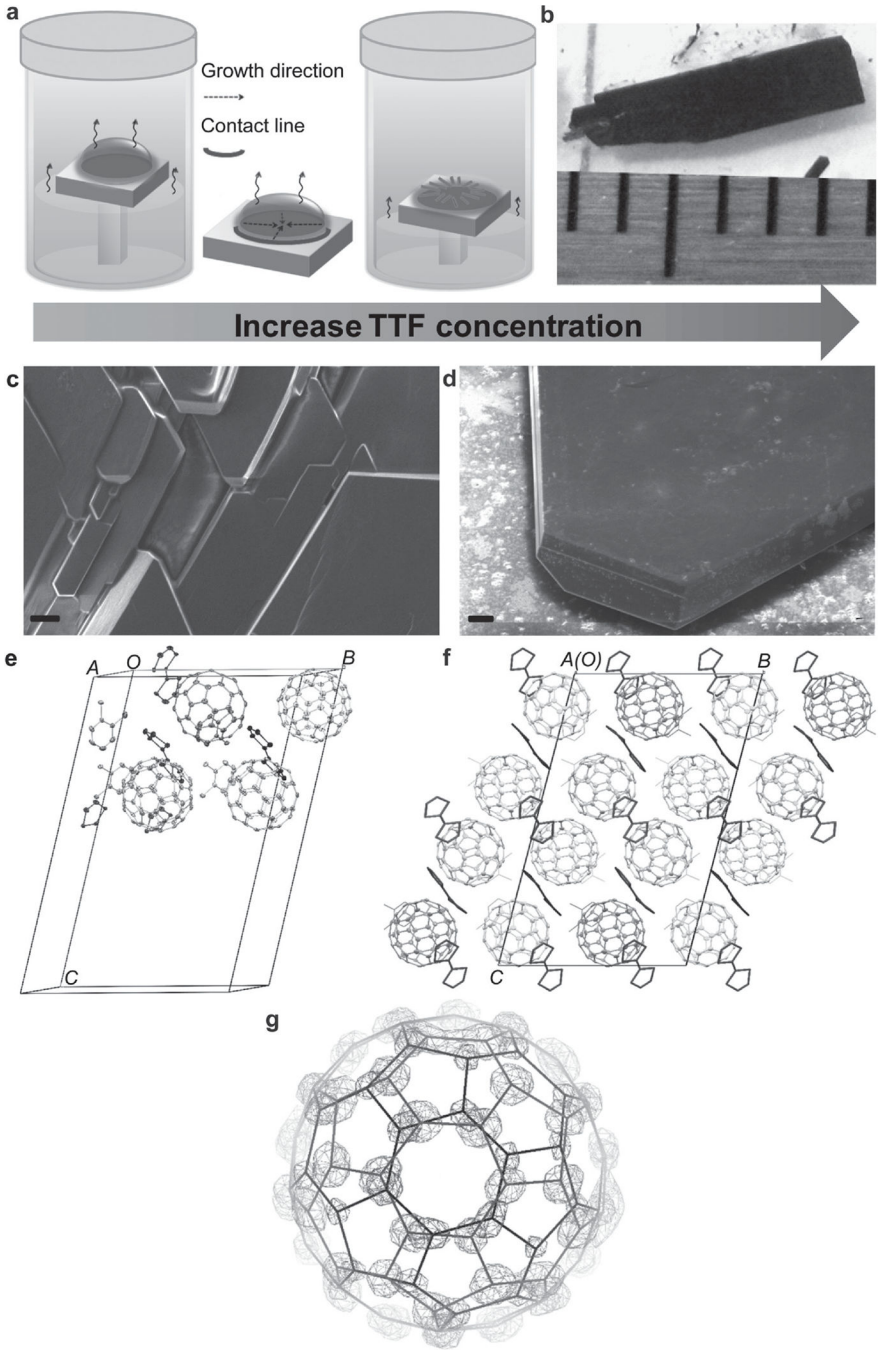

Figure 1.

Schematic illustration of the crystal growth methods, the morphology, structure, and packing of TTF-C_{60} charge-transfer crystals (TCCTs). a) Crystal growth scheme. b) Photograph of TCCTs at the highest concentration of TTF. c,d) SEM images of TCCTs. TTF concentrations are 16.7 and 25 mg mL^{-1}, respectively. The C_{60} concentration is maintained at 25 mg mL^{-1}. The scale bars for SEM images are 10 μm. e) Crystal structure of C_{60}-TTF-DCB complex in an asymmetric unit without disordered parts. The 50% probability ellipsoids of thermal vibrations are shown. The four C_{60} molecules have different

orientations and these are colored in red, cyan, blue, and purple. The crystallographic nonequivalent molecules are shown in different colors. f) Projection of C_{60}-TTF crystal packing along *a* axis. g) Double conformation of C_{60} on the site close to the middle of *b* cell edge created in crystallographic object-oriented toolkit (COOT).[46,48] The high occupancy (0.81) part is presented as blue line with the 2Fo-Fc electron density map in blue mesh at 2σ level. The low occupancy part (0.19) is presented as green line with Fo-Fc difference electron density map in green mesh at 5σ level. The density map was calculated by SHELXL with the minor part omitted and the major part at 0.81 occupacy fixed. Part (e) was drawn by Mercury,[47] the C_{60} molecules are shown as ellipsoids, TTF are shown as sticks, and DCBs are shown as wireframe.

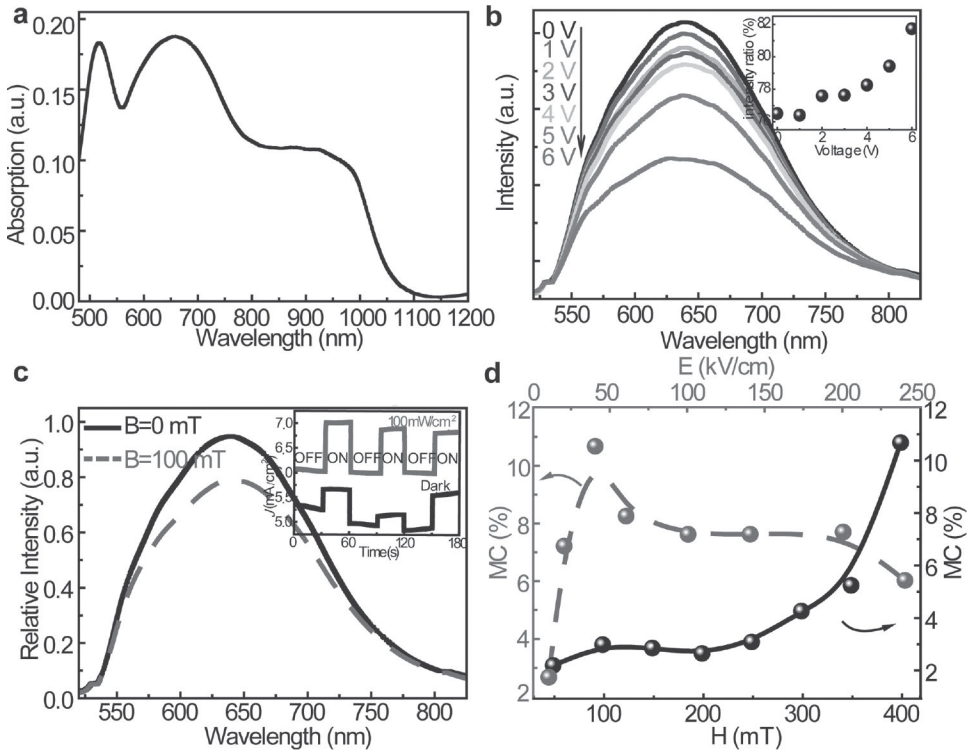

Figure 2.

Optical, electrical properties, magnetic field effect on photoluminescence properties and MC of TCCTs. a) Absorption spectra of TCCTs. b) Potential-dependent photoluminescence spectra for emission polarized at 0° relative to the excitation polarization. The inset in (b) is the ratio of the emission intensities collected at 90° and 0° as a function of applied potential. c) Magnetic-field-dependent photoluminescence spectra at 0° of emission. The inset is the dark and photoexcited MC. d) Electric-field and magnetic-field-dependent MC change, respectively.

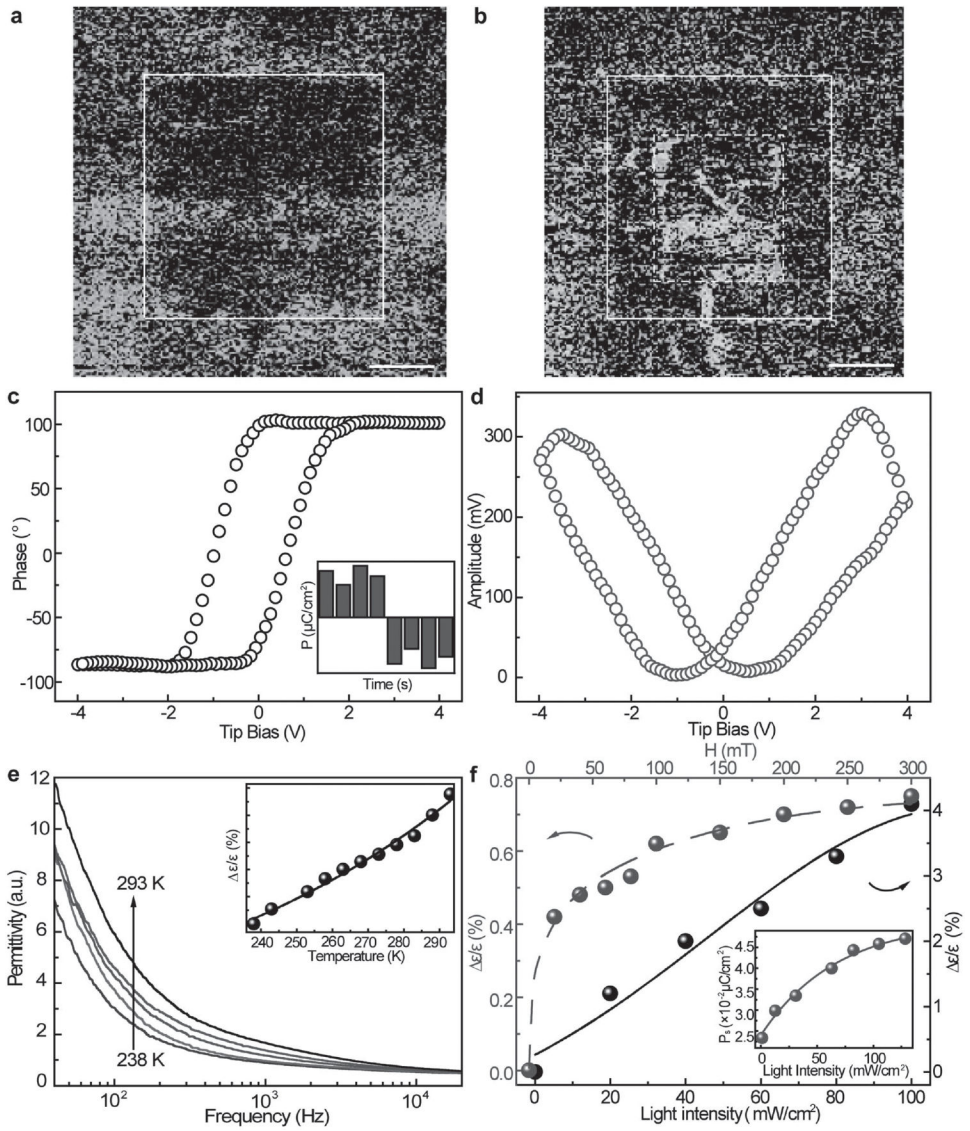

Figure 3.

Ferroelectric and dielectric properties of TCCTs. a,b) Piezoelectric force microscopy image. The square in the center is the polarized area under a voltage of 54 and −72 kV cm^{-1}, respectively. The scale bar is 5 μm. c,d) The phase and amplitude hysteresis loop for piezoelectric response. The inset in (c) is the PUND polarization measurement of TCCTs. e) Frequency-dependent permittivity at different temperatures. The inset is the temperature-dependent permittivity at 100 Hz. f) Magnetic-field and light-intensity-dependent permittivity change. The inset is the light-intensity-dependent polarization value change.

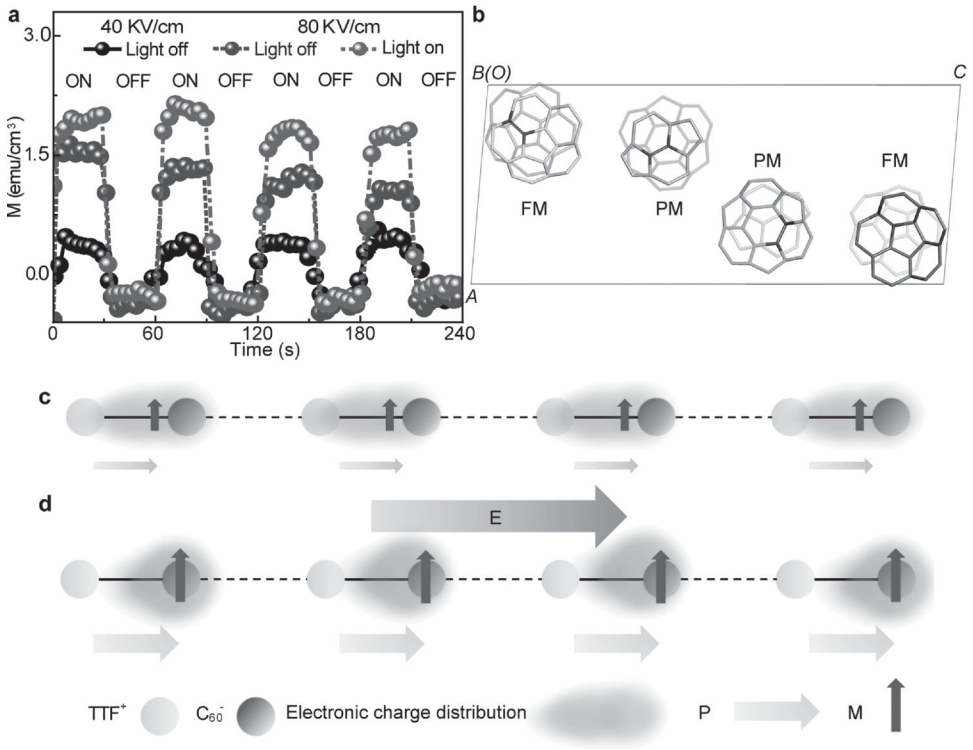

Figure 4.

Magnetism and magnetoelectric coupling properties of TCCTs. a) Electric field tuning of magnetization of TCCTs under dark and photoexcitation conditions at different electric field. The light intensity is 70 mW cm^{-2}. b) The orientations related to ferromeagnetism and paramagnetism by projecting the structure of C_{60} molecules along 010 direction created by *PyMOL*.[48] The 6–6 double bonds in upper layer are colored in red. c) The configurations of charge and spin in TCCTs. The interactions between molecules are presented as 1D chain. Purple circles, shaded yellow ovals, gray arrows, and purple arrows represent molecules, electron distributions, electric dipoles, and spins, respectively, d) The loading of electric field along the chain direction with the enhancement of both polarization and magnetization.